Calculating Geometric Properties of Three-Dimensional Objects from the Spherical Harmonic Representation

Artemy Baxansky and Nahum Kiryati
School of Electrical Engineering
Tel Aviv University
Tel Aviv 69978, Israel

Abstract

The volume, location of the centroid, and second order moments of a three-dimensional star-shaped object are determined in terms of the spherical harmonic coefficients of its boundary function. Bounds on the surface area of the object are derived in terms of the spherical harmonic coefficients as well. Sufficient conditions under which the moments and area computed from the truncated spherical harmonic series converge to the actual moments and area are established. The proposed method is verified using a scanned head model and by recent measurements of the 433 Eros asteroid. An extension to non-star-shaped objects of genus 0 is provided. The computational complexity of our method is shown to be equal to that of the discrete spherical harmonic transform, which is $O(N^2 \log^2 N)$, where N is the maximum order of coefficients retained in the expansion.

1 Introduction

Three-dimensional objects can be represented by surface based descriptions, such as triangular meshes, or by volume based descriptions, such as voxels. These representations, however, are based on huge lists of voxels or surface elements. For purposes of image processing and analysis, the need for a more compact shape representation is important.

Most of this paper is concerned with a limited class of objects called star-shaped. These have the property that there exists a point in the interior of the object from which the whole object is "visible". In this case we can describe the surface of the object using standard spherical coordinates $r = r(\theta, \phi)$. Then r can be arbitrarily well approximated in

the basis of spherical harmonics [3]. Usually the global shape can be captured with a small set of coefficients. It is worth noting that the concept of spherical harmonic representation has been generalized to non-star-shaped objects ([1] and references therein).

The spherical harmonic technique was used to model the heart [18], to approximate molecular orbital surfaces and to compute surface shape properties [6]. Garboczi [8] applied it to characterize aggregate particles in concrete. Spherical harmonics have been also used recently to characterize the shape of an asteriod [20]. In geodesy, they are used to study the shape of the earth and the shape of satellite orbits [10]. In computer vision and graphics, the spherical harmonic representation is the basis for 3D shape matching and retrieval methods [11].

Many applications require the extraction of image-domain features, such as low-order moments and surface area. For example, content-based 3D model retrieval algorithms based on moments have been proposed ([17] and references therein). A possiblity to extract the features directly from the compact representation eliminates the need for prior image reconstruction and may reduce computational complexity. In [13] properties of two-dimensional objects were calculated directly from the Fourier-serier coefficients of the boundary function $r(\phi)$. In this work we extend [13] to the three-dimensional case. The main novelty of this work is that geometric properties are expressed explicitly in terms of the spherical harmonic coefficients.

This paper is organized as follows. In Section 2 we establish some relations that will be applied extensively throughout the paper. In Section 3 we obtain expressions for the moments up to the second order. In Section 4 we develop lower and upper bounds on the surface area. In section 5 we establish sufficient conditions under which the moments and area computed from the partial sums of spherical harmonics converge to the actual

moments and area. Section 6 is concerned with the simulations we performed to verify the theoretical results. As one of the examples, we apply our method to calculate the volume and moments of inertia of the near-Earth asteroid, 433 Eros. In Section 7 we extend our method to non-star-shaped objects of genus 0. In Section 8 we consider the computational complexity of the proposed method comparing two approaches: first, the direct evaluation of a 3D convolution; and second, using the discrete spherical harmonic transform. We show that the former requires $O(N^5)$ operations, as opposed to $O(N^2 \log^2 N)$ for the latter, where N is the maximum order of coefficients retained in the expansion. Finally, conclusions and future work are discussed in Section 9.

2 Preliminaries

Let $\vec{r}$ describe the radius vector directed from the origin to a boundary point of an object. We shall work in spherical coordinates that are natural for describing positions on a sphere. Define ϕ to be the azimuthal angle between the projection of $\vec{r}$ to the xy-plane and the x-axis with $0 \leq \phi \leq 2\pi$, θ to be the polar angle from the z-axis with $0 \leq \theta \leq \pi$, and r to be the distance from the point to the origin (see Figure 1). We label the point on the boundary of the object by its spherical coordinates r, θ, ϕ. If the function $r(\theta, \phi)$ is single-valued, such an object is called star-shaped. $r(\theta, \phi)$ can be expanded into a series of spherical harmonics:

$$r(\theta, \phi) = \sum_{l=0}^{\infty} \sum_{m=-l}^{l} R_{lm} Y_{lm}(\theta, \phi) \tag{1}$$

The spherical harmonics are defined as

$$Y_{lm}(\theta, \phi) = \sqrt{\frac{2l+1}{4\pi} \frac{(l-m)!}{(l+m)!}} P_l^m(\cos\theta) e^{im\phi} \qquad (m \geq 0) \tag{2}$$

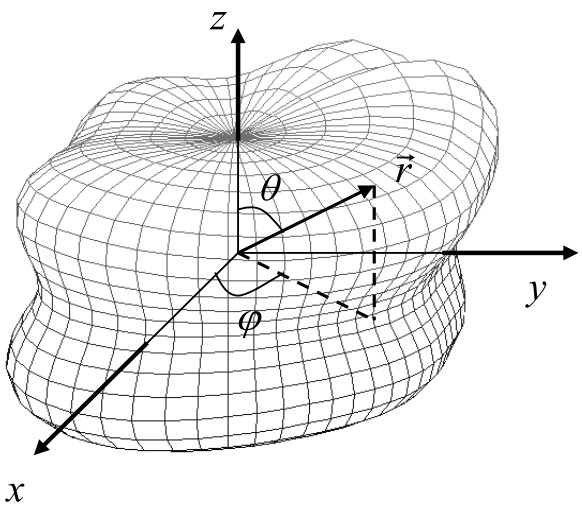

Figure 1: A star-shaped object and the spherical coordinate system

where $P_l^m(\cos\theta)$ are associated Legendre functions, and

$$Y_{l,-m}(\theta,\phi) = (-1)^m Y_{lm}^*(\theta,\phi) \tag{3}$$

The expansion coefficients are given by

$$R_{lm} = \int_{\theta=0}^{\pi}\int_{\phi=0}^{2\pi} r(\theta,\phi) Y_{lm}^*(\theta,\phi)\sin\theta d\theta d\phi \tag{4}$$

For an overview on the properties of spherical harmonics refer, for instance, to [3] (§ D-1-c of chapter VI and complement $\mathrm{A_{VI}}$).

2.1 Extension of the convolution theorem to the 3D case

Given two functions $f(\theta,\phi)$ and $g(\theta,\phi)$ with their spherical harmonic coefficients, $\{A_{lm}\}$ and $\{B_{lm}\}$, respectively, we would like to calculate the coefficients $\{C_{lm}\}$ of $h(\theta,\phi) = f(\theta,\phi)g^*(\theta,\phi)$. According to (4),

$$C_{lm} = \int_{\theta=0}^{\pi} \int_{\phi=0}^{2\pi} h(\theta,\phi) Y^*_{lm}(\theta,\phi) \sin\theta d\theta d\phi$$

$$= \int_{\theta=0}^{\pi} \int_{\phi=0}^{2\pi} \left[\sum_{l_1=0}^{\infty} \sum_{m_1=-l_1}^{l_1} A_{l_1 m_1} Y_{l_1 m_1}(\theta,\phi) \right] \left[\sum_{l_2=0}^{\infty} \sum_{m_2=-l_2}^{l_2} B^*_{l_2 m_2} Y^*_{l_2 m_2}(\theta,\phi) \right] Y^*_{lm}(\theta,\phi) \sin\theta d\theta d\phi$$

Using (3), we may write

$$C_{lm} = \sum_{l_1=0}^{\infty} \sum_{m_1=-l_1}^{l_1} \sum_{l_2=0}^{\infty} \sum_{m_2=-l_2}^{l_2} A_{l_1 m_1} B^*_{l_2 m_2} (-1)^{m_2}$$

$$\times \int_{\theta=0}^{\pi} \int_{\phi=0}^{2\pi} Y_{l_1 m_1}(\theta,\phi) Y_{l_2,-m_2}(\theta,\phi) Y^*_{lm}(\theta,\phi) \sin\theta d\theta d\phi \tag{5}$$

At this point we employ the spherical harmonic addition relation [3], p. 1046:

$$Y_{l_1 m_1}(\theta,\phi) Y_{l_2,-m_2}(\theta,\phi) = \sum_{l'=|l_1-l_2|}^{l_1+l_2} \sum_{m'=-l'}^{l'} \sqrt{\frac{(2l_1+1)(2l_2+1)}{4\pi(2l'+1)}}$$

$$\times \langle l_1, l_2; 0, 0 | l', 0 \rangle \langle l_1, l_2; m_1, -m_2 | l', m' \rangle Y_{l'm'}(\theta,\phi) \tag{6}$$

The coefficients $\langle l_1, l_2; m_1, m_2 | l, m \rangle$ are called Clebsch-Gordan coefficients. They can be calculated by an iterative method. The Clebsch-Gordan coefficient $\langle l_1, l_2; m_1, -m_2 | l', m' \rangle$ is different from zero only if $m' = m_1 - m_2$, therefore the summation over m_2 in (5) is actually unnecessary. Furthermore, the Clebsch-Gordan coefficient $\langle l_1, l_2; 0, 0 | l, 0 \rangle$ is different from zero only if $l_1 + l_2 - l$ is even. Substituting (6) into (5), we find:

$$C_{lm} = \sum_{l_1=0}^{\infty} \sum_{m_1=-l_1}^{l_1} \sum_{l_2=0}^{\infty} \sum_{l'=|l_1-l_2|}^{l_1+l_2} \sum_{m'=-l'}^{l'} A_{l_1 m_1} B^*_{l_2, m_1-m'} (-1)^{m_1-m'} \sqrt{\frac{(2l_1+1)(2l_2+1)}{4\pi(2l'+1)}}$$

$$\times \langle l_1, l_2; 0, 0 | l', 0 \rangle \langle l_1, l_2; m_1, m' - m_1 | l', m' \rangle \int_{\theta=0}^{\pi} \int_{\phi=0}^{2\pi} Y_{l'm'}(\theta, \phi) Y^*_{lm}(\theta, \phi) \sin\theta d\theta d\phi$$

Recall that $\{Y_{lm}\}$ are orthonormal:

$$\int_{\theta=0}^{\pi} \int_{\phi=0}^{2\pi} Y_{l'm'}(\theta, \phi) Y^*_{lm}(\theta, \phi) \sin\theta d\theta d\phi = \delta_{ll',mm'}$$

We therefore have:

$$C_{lm} = \sum_{l_1=0}^{\infty} \sum_{m_1=-l_1}^{l_1} \sum_{l_2=0}^{\infty} A_{l_1 m_1} B^*_{l_2, m_1-m} (-1)^{m_1-m} \sqrt{\frac{(2l_1+1)(2l_2+1)}{4\pi(2l+1)}}$$

$$\times \langle l_1, l_2; 0, 0 | l, 0 \rangle \langle l_1, l_2; m_1, m - m_1 | l, m \rangle \tag{7}$$

In the following we shall use the notation:

$$C_{lm} = A_{lm} * B_{lm} \tag{8}$$

Relation (7) can be viewed as the extension of the convolution theorem well-known from the 2D Fourier series.

2.2 Extension of the Parseval theorem to the 3D case

Consider the integral

$$\int_{\theta=0}^{\pi}\int_{\phi=0}^{2\pi} f(\theta,\phi)g^*(\theta,\phi)\sin\theta d\theta d\phi$$

$$=\sum_{l=0}^{\infty}\sum_{m=-l}^{l}\sum_{l'=0}^{\infty}\sum_{m'=-l'}^{l'} A_{lm}B^*_{l'm'}\int_{\theta=0}^{\pi}\int_{\phi=0}^{2\pi} Y_{lm}(\theta,\phi)Y^*_{l'm'}(\theta,\phi)\sin\theta d\theta d\phi$$

$$=\sum_{l=0}^{\infty}\sum_{m=-l}^{l}\sum_{l'=0}^{\infty}\sum_{m'=-l'}^{l'} A_{lm}B^*_{l'm'}\delta_{ll',mm'}=\sum_{l=0}^{\infty}\sum_{m=-l}^{l} A_{lm}B^*_{lm} \tag{9}$$

where we have used orthonormality of $\{Y_{lm}\}$. This last relation is called the Parseval theorem.

3 Calculation of the Moments of a Figure

3.1 Some auxiliary functions

First let us define some auxiliary functions that will be used in this section and determine their spherical harmonic coefficients. Consider the following functions:

$$s(\theta,\phi)=r^2(\theta,\phi) \tag{10}$$

$$q(\theta,\phi)=r^4(\theta,\phi) \tag{11}$$

$$p(\theta,\phi)=r^5(\theta,\phi) \tag{12}$$

These function can be expanded into spherical harmonic series. Let $\{S_{lm}\}$, $\{Q_{lm}\}$, and $\{P_{lm}\}$ denote the respective sets of spherical harmonic coefficients. They are related with $\{R_{lm}\}$ as

follows. Applying the 3D convolution theorem (8) to $f(\theta,\phi) = g(\theta,\phi) = r(\theta,\phi)$ and using the realness of the radius vector function, we obtain:

$$S_{lm} = R_{lm} * R_{lm} \tag{13}$$

In a similar way, $q(\theta,\phi) = s^2(\theta,\phi)$, therefore we have:

$$Q_{lm} = S_{lm} * S_{lm} \tag{14}$$

Now, since $p(\theta,\phi) = q(\theta,\phi)r(\theta,\phi)$, applying the 3D convolution theorem to $f(\theta,\phi) = q(\theta,\phi)$ and $g(\theta,\phi) = r(\theta,\phi)$, we obtain:

$$P_{lm} = Q_{lm} * R_{lm} \tag{15}$$

3.2 Calculation of the volume

The volume of a figure is given by

$$V = \int_{\rho=0}^{r(\theta,\phi)} \int_{\theta=0}^{\pi} \int_{\phi=0}^{2\pi} \rho^2 \sin\theta d\rho d\theta d\phi = \frac{1}{3} \int_{\theta=0}^{\pi} \int_{\phi=0}^{2\pi} r^3(\theta,\phi) \sin\theta d\theta d\phi \tag{16}$$

Note that we can represent $r^3(\theta,\phi)$ as $s(\theta,\phi)r(\theta,\phi)$. Substituting $f(\theta,\phi) = s(\theta,\phi)$ and $g(\theta,\phi) = r(\theta,\phi)$ into the Parseval relation (9) yields:

$$V = \frac{1}{3} \int_{\theta=0}^{\pi} \int_{\phi=0}^{2\pi} s(\theta,\phi)r(\theta,\phi) \sin\theta d\theta d\phi = \frac{1}{3} \sum_{l=0}^{\infty} \sum_{m=-l}^{l} S_{lm} R^*_{lm} \tag{17}$$

As we can see from the last equation, the volume of a figure can be calculated from $\{R_{lm}\}$ and $\{S_{lm}\}$, which are the spherical harmonic coefficients of the boundary function $r(\theta,\phi)$

and its square, respectively. Since $\{S_{lm}\}$ can be obtained from $\{R_{lm}\}$ using the 3D convolution theorem, we conclude that to calculate the volume one basically needs to perform a convolution operation.

3.3 Calculation of the centroid

Let $(\bar{x}, \bar{y}, \bar{z})$ denote the coordinates of the centroid of a region. The x-coordinate of the centroid is given by

$$\bar{x} = \frac{1}{V}\int_{Object} x dv = \frac{1}{V}\int_{\rho=0}^{r(\theta,\phi)}\int_{\theta=0}^{\pi}\int_{\phi=0}^{2\pi}(\rho\sin\theta\cos\phi)\rho^2\sin\theta d\rho d\theta d\phi$$

$$= \frac{1}{4V}\int_{\theta=0}^{\pi}\int_{\phi=0}^{2\pi} r^4(\theta,\phi)\sin\theta\cos\phi\sin\theta d\theta d\phi \tag{18}$$

Next we express $(\sin\theta\cos\phi)$ as a series of spherical harmonics. We can write:

$$\sin\theta\cos\phi = \frac{1}{2}(\sin\theta e^{i\phi} + \sin\theta e^{-i\phi})$$

Note that (for example, see [14], p. 386):

$$Y_{1,1}(\theta,\phi) = -\sqrt{\frac{3}{8\pi}}\sin\theta e^{i\phi} \tag{19}$$

$$Y_{1,-1}(\theta,\phi) = \sqrt{\frac{3}{8\pi}}\sin\theta e^{-i\phi} \tag{20}$$

Thus,

$$\sin\theta\cos\phi = \sqrt{\frac{2\pi}{3}}\left[Y_{1,-1}(\theta,\phi) - Y_{1,1}(\theta,\phi)\right] \tag{21}$$

We apply (9) to $f(\theta,\phi) = r^4(\theta,\phi)$ and $g(\theta,\phi) = \sin\theta\cos\phi$ to get

$$\bar{x} = \frac{1}{4V}\sqrt{\frac{2\pi}{3}}\,(Q_{1,-1} - Q_{1,1}) \tag{22}$$

In the last equation $Q_{1,-1}$ and $Q_{1,1}$ are the spherical harmonic coefficients of $r^4(\theta,\phi)$ corresponding to $(l,m) = (1,-1)$ and $(1,1)$, respectively. Proceeding similarly, we have for the y-coordinate of the centroid:

$$\bar{y} = \frac{1}{V}\int_{Object} y dv = \frac{1}{V}\int_{\rho=0}^{r(\theta,\phi)}\int_{\theta=0}^{\pi}\int_{\phi=0}^{2\pi}(\rho\sin\theta\sin\phi)\rho^2\sin\theta d\rho d\theta d\phi$$

$$= \frac{1}{4V}\int_{\theta=0}^{\pi}\int_{\phi=0}^{2\pi} r^4(\theta,\phi)\sin\theta\sin\phi\sin\theta d\theta d\phi$$

Like previously, we expand $(\sin\theta\sin\phi)$ in a series of spherical harmonics:

$$\sin\theta\sin\phi = \frac{1}{2i}(\sin\theta e^{i\phi} - \sin\theta e^{-i\phi}) = i\sqrt{\frac{2\pi}{3}}\,[Y_{1,-1}(\theta,\phi) + Y_{1,1}(\theta,\phi)] \tag{23}$$

where the last equality follows from (19) and (20). Substituting $f(\theta,\phi) = r^4(\theta,\phi)$ and $g(\theta,\phi) = \sin\theta\sin\phi$ into (9) gives:

$$\bar{y} = \frac{i}{4V}\sqrt{\frac{2\pi}{3}}(Q_{1,-1} + Q_{1,1}) \tag{24}$$

Finally, the z-coordinate of the centroid can be written as

$$\bar{z} = \frac{1}{V}\int_{Object} z dv = \frac{1}{V}\int_{\rho=0}^{r(\theta,\phi)}\int_{\theta=0}^{\pi}\int_{\phi=0}^{2\pi}(\rho\cos\theta)\rho^2\sin\theta d\rho d\theta d\phi$$

$$= \frac{1}{4V} \int_{\theta=0}^{\pi} \int_{\phi=0}^{2\pi} r^4(\theta, \phi) \cos\theta \sin\theta d\theta d\phi$$

Note that ([14], p. 386):

$$Y_{1,0}(\theta, \phi) = \sqrt{\frac{3}{4\pi}} \cos\theta$$

Therefore

$$cos\theta = \sqrt{\frac{4\pi}{3}} Y_{1,0}(\theta, \phi) \tag{25}$$

Now we apply (9) to $f(\theta, \phi) = r^4(\theta, \phi)$ and $g(\theta, \phi) = \cos\theta$ to get

$$\bar{z} = \frac{1}{2V} \sqrt{\frac{\pi}{3}} Q_{1,0} \tag{26}$$

Here $Q_{1,0}$ is the spherical harmonic coefficient of $r^4(\theta, \phi)$ corresponding to $(l, m) = (1, 0)$. We have thus shown that in order to obtain the centroid of a figure, it is sufficient to know $\{Q_{lm}\}$, the spherical harmonic coefficients of $r^4(\theta, \phi)$. $\{Q_{lm}\}$ can be computed by means of the 3D convolution theorem from the coefficients of $r^2(\theta, \phi)$, which are, in turn, can be computed from the coefficients of $r(\theta, \phi)$. It follows that calculating the centroid of a figure requires two convolution operations.

3.4 Calculation of the second order moments

Let us define the second-order moments of a figure as

$$M_{ij} = \int_{Object} ijdv$$

where each of the variables i and j stand for x, y, or z. The xx-moment can be written in the form

$$M_{xx} = \int_{Object} x^2 dv = \int_{\rho=0}^{r(\theta,\phi)} \int_{\theta=0}^{\pi} \int_{\phi=0}^{2\pi} (\rho \sin\theta \cos\phi)^2 \rho^2 \sin\theta d\rho d\theta d\phi$$

$$= \frac{1}{5} \int_{\theta=0}^{\pi} \int_{\phi=0}^{2\pi} r^5(\theta,\phi) (\sin\theta \cos\phi)^2 \sin\theta d\theta d\phi$$

Like we did in Section 3.3, we need to express $(\sin\theta\cos\phi)^2$ as a linear combination of spherical harmonics. Applying the 3D convolution theorem (8) to $f(\theta,\phi) = g(\theta,\phi) = \sin\theta\cos\phi$ and using (21) we obtain:

$$(\sin\theta\cos\phi)^2 = C_{0,0}^{(xx)} Y_{0,0}(\theta,\phi) + C_{2,-2}^{(xx)} Y_{2,-2}(\theta,\phi) + C_{2,0}^{(xx)} Y_{2,0}(\theta,\phi) + C_{2,2}^{(xx)} Y_{2,2}(\theta,\phi)$$

where the coefficients of this expansion are given in terms of the corresponding Clebsch-Gordan coefficients as follows:

$$C_{0,0}^{(xx)} = -2\sqrt{\pi} \langle 1,1;0,0|0,0\rangle \langle 1,1;1,-1|0,0\rangle$$

$$C_{2,-2}^{(xx)} = \sqrt{\frac{\pi}{5}} \langle 1,1;0,0|2,0\rangle \langle 1,1;-1,-1|2,-2\rangle$$

$$C_{2,0}^{(xx)} = -2\sqrt{\frac{\pi}{5}} \langle 1,1;0,0|2,0\rangle \langle 1,1;1,-1|2,0\rangle$$

$$C_{2,2}^{(xx)} = \sqrt{\frac{\pi}{5}} \langle 1,1;0,0|2,0\rangle \langle 1,1;1,1|2,2\rangle$$

Now using the Parseval theorem we get:

$$M_{xx} = \frac{1}{5}\left(C_{0,0}^{(xx)}P_{0,0} + C_{2,-2}^{(xx)}P_{2,-2} + C_{2,0}^{(xx)}P_{2,0} + C_{2,2}^{(xx)}P_{2,2}\right) \tag{27}$$

The rest of the second-order moments can be calculated in a similar way. Exact expressions for them are derived in the Appendix. We have therefore shown that the second-order moments of a figure can be expressed in terms of $\{P_{lm}\}$, which are the spherical harmonic coefficients of $r^5(\theta, \phi)$. According to Section 3.1, $\{P_{lm}\}$ can be computed from $\{Q_{lm}\}$ and $\{R_{lm}\}$ by means of the 3D convolution theorem. Calculating $\{Q_{lm}\}$, in turn, requires two convolution operations. It follows that to calculate the second-order moments, we need to perform three convolution operations. Once we have calculated M_{ij}, the elements of the inertia tensor can be expressed in terms of M_{ij} as well.

It can be seen that the above method can also be applied to higher order moments. A moment of any order can be written as an integral over the whole spherical angle so that the expression under the integral sign is a product of some power of r and some trigonometric function. To obtain the value of a moment, we need to compute the spherical harmonic coefficients of the power of r by the repetitive application of the 3D convolution theorem, expand the trigonometric function into a series of spherical harmonics, and finally use the Parseval relation.

4 Bounds on the Surface Area of a Figure

Given the radius vector $\vec{r}(\theta, \phi)$, the surface area of a figure can be expressed as

$$A = \int_{\theta=0}^{\pi}\int_{\phi=0}^{2\pi}\left|\frac{\partial\vec{r}}{\partial\theta} \times \frac{\partial\vec{r}}{\partial\phi}\right| d\theta d\phi \tag{28}$$

Let us denote by $\hat{r}$, $\hat{\theta}$, and $\hat{\phi}$ the unit vectors in the radial, polar, and azimuthal directions, respectively. We can write

$$\vec{r} = r\hat{r}$$

Therefore

$$\frac{\partial \vec{r}}{\partial \theta} = \frac{\partial r}{\partial \theta}\hat{r} + r\frac{\partial \hat{r}}{\partial \theta}$$

Recalling that

$$\hat{r} = (\sin\theta\cos\phi)\hat{x} + (\sin\theta\sin\phi)\hat{y} + (\cos\theta)\hat{z} \tag{29}$$

we obtain

$$\frac{\partial \hat{r}}{\partial \theta} = (\cos\theta\cos\phi)\hat{x} + (\cos\theta\sin\phi)\hat{y} - (\sin\theta)\hat{z} = \hat{\theta}$$

In a similar way

$$\frac{\partial \vec{r}}{\partial \phi} = \frac{\partial r}{\partial \phi}\hat{r} + r\frac{\partial \hat{r}}{\partial \phi}$$

It follows from (29) that

$$\frac{\partial \hat{r}}{\partial \phi} = -(\sin\theta\sin\phi)\hat{x} + (\sin\theta\cos\phi)\hat{y} = (\sin\theta)\hat{\phi}$$

We see that:

$$\vec{r}_\theta \times \vec{r}_\phi = \begin{vmatrix} \hat{r} & \hat{\theta} & \hat{\phi} \\ r_\theta & r & 0 \\ r_\phi & 0 & r\sin\theta \end{vmatrix} = (r^2\sin\theta)\hat{r} - (rr_\theta\sin\theta)\hat{\theta} - (rr_\phi)\hat{\phi} \tag{30}$$

Note that the determinant formula for the cross product is well known in the Cartesian coordinates. To see why it is applicable in the spherical coordinates, recall that the cross product is independent of the coordinate system. At the point the cross product is evaluated, the unit vectors $\hat{r}$, $\hat{\theta}$, and $\hat{\phi}$ form a right-hand orthogonal axis system, just as $\hat{x}$, $\hat{y}$, and $\hat{z}$ do. Since the determinant formula for the cross product is obtained by a term-by-term multiplication between the components of the two vectors, it is valid for every right-hand orthogonal system. Now let us define

$$B_1 = r^2\sin\theta \tag{31}$$

$$B_2 = rr_\theta\sin\theta \tag{32}$$

$$B_3 = rr_\phi \tag{33}$$

Substituting (30) into (28) and taking into account (31-33), we obtain:

$$A = \int_{\theta=0}^{\pi}\int_{\phi=0}^{2\pi}\sqrt{B_1^2 + B_2^2 + B_3^2}d\theta d\phi \tag{34}$$

We see that the last equation involves a square root. That prevents us from deriving an exact expression for the surface area in terms of the spherical harmonic coefficients $\{R_{lm}\}$. It is possible, however, to derive useful bounds that can be expressed explicitly in terms of

$\{R_{lm}\}$. In the rest of this section, we shall develop lower and upper bounds on the surface area using the last equation as a starting point.

4.1 Lower bounds on the surface area

We shall follow the approach similar to that used in [13]. Formula (34) can be written in the form:

$$A = \int_{\theta=0}^{\pi} \int_{\phi=0}^{2\pi} \left| \sqrt{B_1^2 + B_2^2} + jB_3 \right| d\theta d\phi$$

$$= \int_{\theta=0}^{\pi} \int_{\phi=0}^{2\pi} ||B_1 + jB_2| + jB_3| \, d\theta d\phi$$

Let us denote by $\{\Omega_k\}$ some partition of the sphere, i.e. $\bigcup_k \Omega_k = \{(\theta, \phi) : 0 \leq \theta \leq \pi, 0 \leq \phi \leq 2\pi\}$ and $\Omega_i \bigcap \Omega_j = 0$ for $i \neq j$. Then we get

$$A = \sum_k \iint_{\Omega_k} ||B_1 + jB_2| + jB_3| \, d\theta d\phi \tag{35}$$

We can now write the string of inequalities:

$$\iint_{\Omega_k} ||B_1 + jB_2| + jB_3| \, d\theta d\phi \geq \iint_{\Omega_k} \max\left(|B_1 + jB_2|, |B_3|\right) d\theta d\phi$$

$$\geq \max\left(\iint_{\Omega_k} |B_1 + jB_2| d\theta d\phi, \iint_{\Omega_k} |B_3| d\theta d\phi \right)$$

$$\geq \max\left(\iint_{\Omega_k} \max\left(|B_1|, |B_2|\right) d\theta d\phi, \iint_{\Omega_k} |B_3| d\theta d\phi \right)$$

$$\geq \max\left[\max\left(\iint_{\Omega_k}|B_1|d\theta d\phi, \iint_{\Omega_k}|B_2|d\theta d\phi\right), \iint_{\Omega_k}|B_3|d\theta d\phi\right]$$

$$\geq \max\left(\iint_{\Omega_k}|B_1|d\theta d\phi, \iint_{\Omega_k}|B_2|d\theta d\phi, \iint_{\Omega_k}|B_3|d\theta d\phi\right)$$

$$\geq \max\left(\left|\iint_{\Omega_k}B_1 d\theta d\phi\right|, \left|\iint_{\Omega_k}B_2 d\theta d\phi\right|, \left|\iint_{\Omega_k}B_3 d\theta d\phi\right|\right) \tag{36}$$

The first of the integrals on the right-hand side of (36) is given by

$$\iint_{\Omega_k}B_1 d\theta d\phi = \iint_{\Omega_k}r^2(\theta,\phi)\sin\theta d\theta d\phi = \iint_{\Omega_k}\left[\sum_{l=0}^{\infty}\sum_{m=-l}^{l}S_{lm}Y_{lm}(\theta,\phi)\right]\sin\theta d\theta d\phi$$

where $\{S_{lm}\}$ are the spherical harmonic coefficients of $r^2(\theta,\phi)$ that were calculated in Section 3.1. Let us denote

$$J_{lm}(\Omega_k) = \iint_{\Omega_k}Y_{lm}(\theta,\phi)\sin\theta d\theta d\phi \tag{37}$$

The integrals $J_{lm}(\Omega_k)$ can be computed off-line using numerical methods. It follows that

$$\iint_{\Omega_k}B_1 d\theta d\phi = \sum_{l=0}^{\infty}\sum_{m=-l}^{l}S_{lm}J_{lm}(\Omega_k) \tag{38}$$

We proceed by calculating the spherical harmonic coefficients $\{T_{lm}\}$ of $B_2 = rr_\theta\sin\theta$. We have

$$\sin\theta\frac{dP_l^m(\cos\theta)}{d\theta} = \sin\theta\frac{dP_l^m(\cos\theta)}{d(\cos\theta)}(-\sin\theta) = -(1-x^2)\frac{dP_l^m(x)}{dx}\bigg|_{x=\cos\theta}$$

Applying the recurrence relation [14], p. 388

$$(1-x^2)\frac{dP_l^m(x)}{dx} = (l+1)xP_l^m(x) - (l-m+1)P_{l+1}^m(x) \tag{39}$$

we obtain

$$\sin\theta\frac{dP_l^m(\cos\theta)}{d\theta} = -(l+1)\cos\theta P_l^m(\cos\theta) + (l-m+1)P_{l+1}^m(\cos\theta) \tag{40}$$

Consequently, using the definition of spherical harmonics with a non-negative azimuthal number m in eq. (2), we can write for $m \geq 0$

$$\frac{\partial Y_{lm}(\theta,\phi)}{\partial\theta}\sin\theta = \sqrt{\frac{2l+1}{4\pi}\frac{(l-m)!}{(l+m)!}}e^{im\phi}\sin\theta\frac{dP_l^m(\cos\theta)}{d\theta}$$

$$= \sqrt{\frac{2l+1}{4\pi}\frac{(l-m)!}{(l+m)!}}e^{im\phi}\left[-(l+1)\cos\theta P_l^m(\cos\theta) + (l-m+1)P_{l+1}^m(\cos\theta)\right]$$

$$= -(l+1)\cos\theta Y_{lm}(\theta,\phi) + \sqrt{\frac{2l+1}{2(l+1)+1}(l+m+1)(l-m+1)}Y_{l+1,m}(\theta,\phi) \tag{41}$$

In a similar way, using the definition of spherical harmonics with a negative azimuthal number in eq. (3), we can write for $m \geq 0$

$$\frac{\partial Y_{l,-m}(\theta,\phi)}{\partial\theta}\sin\theta = (-1)^m\frac{\partial Y_{l,m}^*(\theta,\phi)}{\partial\theta}\sin\theta$$

$$= -(l+1)\cos\theta(-1)^m Y_{lm}^*(\theta,\phi) + \sqrt{\frac{2l+1}{2(l+1)+1}(l+m+1)(l-m+1)}(-1)^m Y_{l+1,m}^*(\theta,\phi)$$

$$= -(l+1)\cos\theta Y_{l,-m}(\theta,\phi) + \sqrt{\frac{2l+1}{2(l+1)+1}(l+m+1)(l-m+1)}Y_{l+1,-m}(\theta,\phi) \tag{42}$$

Inspecting eq. (42), we notice that it has the same form as (41), except that m is replaced with $-m$. That actually means that (41) holds for both non-negative and negative m. Now, $r_\theta \sin\theta$ can be expressed as

$$r_\theta \sin\theta = \sum_{l=0}^{\infty}\sum_{m=-l}^{l} R_{lm}\frac{\partial Y_{lm}(\theta,\phi)}{\partial\theta}\sin\theta \tag{43}$$

Let

$$t_1(\theta,\phi) = -\cos\theta\sum_{l=0}^{\infty}\sum_{m=-l}^{l}(l+1)R_{lm}Y_{lm}(\theta,\phi) \tag{44}$$

and

$$t_2(\theta,\phi) = \sum_{l=0}^{\infty}\sum_{m=-l}^{l}\sqrt{\frac{2l+1}{2(l+1)+1}(l+m+1)(l-m+1)}R_{lm}Y_{l+1,m}(\theta,\phi) \tag{45}$$

Then (43) together with (41) yields:

$$r_\theta \sin\theta = t_1(\theta,\phi) + t_2(\theta,\phi) \tag{46}$$

Let $\{T_{lm}^{(1)}\}$ and $\{T_{lm}^{(2)}\}$ be the spherical harmonic coefficients of $t_1(\theta,\phi)$ and $t_2(\theta,\phi)$, respectively. Applying the 3D convolution theorem (7) to $f(\theta,\phi) = \sum_{l=0}^{\infty}\sum_{m=-l}^{l}(l+1)R_{lm}Y_{lm}(\theta,\phi)$ and $g(\theta,\phi) = \cos\theta$ and using the spherical harmonic representation of $\cos\theta$ (25), it can be shown that:

$$T_{lm}^{(1)} = -\sum_{l_1=\max(|l-1|,|m|)}^{l+1} (l_1+1) R_{l_1 m} \sqrt{\frac{2l_1+1}{2l+1}} \langle l_1, 1; 0, 0 | l, 0 \rangle \langle l_1, 1; m, 0 | l, m \rangle \tag{47}$$

Obviously

$$T_{lm}^{(2)} = \begin{cases} \sqrt{\frac{2l-1}{2l+1}(l^2-m^2)} R_{l-1,m} & \text{if } l \geq 1 \text{ and } -(l-1) \leq m \leq l-1 \\ 0 & \text{otherwise} \end{cases} \tag{48}$$

Finally, applying (8) to $f(\theta, \phi) = r(\theta, \phi)$ and $g(\theta, \phi) = r_\theta \sin\theta$ and using (46), we see that the spherical harmonic coefficients $\{T_{lm}\}$ of $B_2 = r r_\theta \sin\theta$ are given by

$$T_{lm} = R_{lm} * (T_{lm}^{(1)} + T_{lm}^{(2)}) \tag{49}$$

Now, the second integral on the right-hand side of (36) is given by

$$\iint_{\Omega_k} B_2 d\theta d\phi = \iint_{\Omega_k} \left[\sum_{l=0}^{\infty} \sum_{m=-l}^{l} T_{lm} Y_{lm}(\theta, \phi) \right] d\theta d\phi$$

Define

$$I_{lm}(\Omega_k) = \iint_{\Omega_k} Y_{lm}(\theta, \phi) d\theta d\phi \tag{50}$$

The integrals $I_{lm}(\Omega_k)$ can be calculated off-line numerically, like $J_{lm}(\Omega_k)$. We conclude that:

$$\iint_{\Omega_k} B_2 d\theta d\phi = \sum_{l=0}^{\infty} \sum_{m=-l}^{l} T_{lm} I_{lm}(\Omega_k) \tag{51}$$

Next let us calculate the spherical harmonic coefficients $\{F_{lm}\}$ of $r r_\phi$. From the definition of spherical harmonics (2-3) we have:

$$\frac{\partial Y_{lm}(\theta,\phi)}{\partial \phi} = imY_{lm}(\theta,\phi)$$

Therefore

$$r_\phi = \sum_{l=0}^{\infty}\sum_{m=-l}^{l} R_{lm}\frac{\partial Y_{lm}(\theta,\phi)}{\partial \phi} = i\sum_{l=0}^{\infty}\sum_{m=-l}^{l} mR_{lm}Y_{lm}(\theta,\phi)$$

Applying (8) to $f(\theta,\phi) = r(\theta,\phi)$ and $g(\theta,\phi) = r_\phi$ and using the last equation, we get:

$$F_{lm} = R_{lm} * (imR_{lm}) \tag{52}$$

This leads us to conclude that the third integral on the right-hand side of (36) is given by:

$$\iint_{\Omega_k} B_3 d\theta d\phi = \iint_{\Omega_k}\left[\sum_{l=0}^{\infty}\sum_{m=-l}^{l} F_{lm}Y_{lm}(\theta,\phi)\right] d\theta d\phi = \sum_{l=0}^{\infty}\sum_{m=-l}^{l} F_{lm}I_{lm}(\Omega_k) \tag{53}$$

A lower bound on A is obtained by combining (35), (36), (38), (51), and (53). Various choices of the partion $\{\Omega_k\}$ lead to various bounds. In general, as our partition gets finer and finer, we get tighter bounds, while the amount of computation and storage increases.

4.2 Upper bound on the surface area

We shall use the Cauchy-Schwarz inequality for integrals:

$$\left[\int_{\theta=0}^{\pi}\int_{\phi=0}^{2\pi} f(\theta,\phi)g(\theta,\phi)d\theta d\phi\right]^2 \leq \left\{\int_{\theta=0}^{\pi}\int_{\phi=0}^{2\pi}\left[f(\theta,\phi)\right]^2 d\theta d\phi\right\}\left\{\int_{\theta=0}^{\pi}\int_{\phi=0}^{2\pi}\left[g(\theta,\phi)\right]^2 d\theta d\phi\right\}$$

Substituting $f(\theta,\phi) = \sqrt{B_1^2 + B_2^2 + B_3^2}$ and $g(\theta,\phi) = 1$ and taking into account (34), we get

$$A^2 \leq 2\pi^2 \int_{\theta=0}^{\pi} \int_{\phi=0}^{2\pi} (B_1^2 + B_2^2 + B_3^2) d\theta d\phi \tag{54}$$

The first term on the right-hand side of (54) is given by

$$\int_{\theta=0}^{\pi} \int_{\phi=0}^{2\pi} B_1^2 d\theta d\phi = \int_{\theta=0}^{\pi} \int_{\phi=0}^{2\pi} r^4(\theta, \phi) \sin^2 \theta d\theta d\phi$$

$$= \int_{\theta=0}^{\pi} \int_{\phi=0}^{2\pi} \left[\sum_{l=0}^{\infty} \sum_{m=-l}^{l} Q_{lm} Y_{lm}(\theta, \phi) \right] \sin^2 \theta d\theta d\phi$$

Define

$$K_{lm} = \int_{\theta=0}^{\pi} \int_{\phi=0}^{2\pi} Y_{lm}(\theta, \phi) \sin^2 \theta d\theta d\phi \tag{55}$$

The integrals K_{lm} can be calculated off-line using numerical methods, like $I_{lm}(\Omega_k)$ and $J_{lm}(\Omega_k)$. Noting that $K_{lm} \neq 0$ only for $m = 0$, we can write

$$\int_{\theta=0}^{\pi} \int_{\phi=0}^{2\pi} B_1^2 d\theta d\phi = \sum_{l=0}^{\infty} Q_{l,0} K_{l,0} \tag{56}$$

Let $\{T_{lm}^{(2)}\}$ be the spherical harmonic coefficients of B_2^2. According to (8)

$$T_{lm}^{(2)} = T_{lm} * T_{lm}$$

where $\{T_{lm}\}$ can be calculated by combining (47-49). Hence the second term on the right-hand side of (54) can be written in the form

$$\int_{\theta=0}^{\pi} \int_{\phi=0}^{2\pi} B_2^2 d\theta d\phi = \int_{\theta=0}^{\pi} \int_{\phi=0}^{2\pi} \left[\sum_{l=0}^{\infty} \sum_{m=-l}^{l} T_{lm}^{(2)} Y_{lm}(\theta, \phi) \right] d\theta d\phi$$

$$= \sum_{l=0}^{\infty} T_{l,0}^{(2)} I_{l,0}(\Omega) \tag{57}$$

where we have used the definition in (50) and the fact that $I_{lm}(\Omega)$ is different from zero only for $m = 0$. Let $\{F_{lm}^{(2)}\}$ be the spherical harmonic coefficients of B_3^2. According to (8)

$$F_{lm}^{(2)} = F_{lm} * F_{lm}$$

where $\{F_{lm}\}$ were calculated in (52). Therefore the third term on the right-hand side of (54), similarly to the second one, is given by

$$\int_{\theta=0}^{\pi} \int_{\phi=0}^{2\pi} B_3^2 d\theta d\phi = \int_{\theta=0}^{\pi} \int_{\phi=0}^{2\pi} \left[\sum_{l=0}^{\infty} \sum_{m=-l}^{l} F_{lm}^{(2)} Y_{lm}(\theta, \phi) \right] d\theta d\phi$$

$$= \sum_{l=0}^{\infty} F_{l,0}^{(2)} I_{l,0}(\Omega) \tag{58}$$

The upper bound on A is obtained by combining (54) and (56-58).

5 Proof of Convergence

The question arises as to under which conditions the moments and area computed from the truncated spherical harmonic series converge to the actual moments and area. Define

$$r_n(\theta, \phi) = \sum_{l=-n}^{n} \sum_{m=-l}^{l} R_{lm} Y_{lm}(\theta, \phi)$$

We show that

1. If the function $r(\theta, \phi)$ is continuously differentiable, then the sequence of moments

computed from $r_n(\theta,\phi)$ converges to the actual moment.

2. If the partial derivatives $\frac{\partial r}{\partial \theta}$ and $\frac{\partial r}{\partial \phi}$ are continuously differentiable, then the sequence of surface areas computed from $r_n(\theta,\phi)$ converges to the actual surface area.

We shall start with the volume of a figure. Bearing in mind the expression of V given in (16) we denote

$$f(\theta,\phi)=\frac{1}{3}r^3(\theta,\phi) \tag{59}$$

$$f_n(\theta,\phi)=\frac{1}{3}{r_n}^3(\theta,\phi) \tag{60}$$

Let V_n be the volume of the figure described by $r_n(\theta,\phi)$. We have

$$|V_n-V|=\left|\int_{\theta=0}^{\pi}\int_{\phi=0}^{2\pi}[f_n(\theta,\phi)-f(\theta,\phi)]\sin\theta d\theta d\phi\right|$$

According to the triangle inequality

$$|V_n-V|\leq\int_{\theta=0}^{\pi}\int_{\phi=0}^{2\pi}|f_n(\theta,\phi)-f(\theta,\phi)|\sin\theta d\theta d\phi \tag{61}$$

It is proved in [12], p. 259 that if $r(\theta,\phi)$ is continuously differentiable, then it is developable in a uniformly convergent series of spherical harmonics. In other words, for any $\epsilon>0$ there exists N such that for every $n>N$ and every θ and ϕ

$$|r_n(\theta,\phi)-r(\theta,\phi)|<\epsilon$$

Next we shall need the following lemma.

Lemma. *Consider two bounded functions $f(\theta,\phi)$ and $g(\theta,\phi)$ defined on $0\leq\theta\leq\pi$,*

$0 \leq \phi \leq 2\pi$. *If the sequences of functions* $f_n(\theta, \phi)$ *and* $g_n(\theta, \phi)$ *converge uniformly to* $f(\theta, \phi)$ *and* $g(\theta, \phi)$*, respectively, then the sequence* $h_n(\theta, \phi) = f_n(\theta, \phi)g_n(\theta, \phi)$ *converges uniformly to* $h(\theta, \phi) = f(\theta, \phi)g(\theta, \phi)$.

Proof. We may write

$$|h_n(\theta, \phi) - h(\theta, \phi)|$$

$$= |[f(\theta, \phi) + f_n(\theta, \phi) - f(\theta, \phi)]\,[g(\theta, \phi) + g_n(\theta, \phi) - g(\theta, \phi)] - f(\theta, \phi)g(\theta, \phi)|$$

$$\leq |f_n(\theta, \phi) - f(\theta, \phi)|\,|g(\theta, \phi)| + |f(\theta, \phi)|\,|g_n(\theta, \phi) - g(\theta, \phi)|$$

$$+ |f_n(\theta, \phi) - f(\theta, \phi)|\,|g_n(\theta, \phi) - g(\theta, \phi)|$$

$f(\theta, \phi)$ and $g(\theta, \phi)$ are bounded, i.e. there exist positive numbers M_1 and M_2 such that for every θ and ϕ it holds that $|f(\theta, \phi)| < M_1$ and $|g(\theta, \phi)| < M_2$. Since $f_n(\theta, \phi)$ converge uniformly to $f(\theta, \phi)$, for any $\delta > 0$ there exists N_1 such that for every $n > N_1$ and every θ and ϕ

$$|f_n(\theta, \phi) - f(\theta, \phi)| < \delta$$

Similarly, for any $\delta > 0$ there exists N_2 such that for every $n > N_2$ and every θ and ϕ

$$|g_n(\theta, \phi) - g(\theta, \phi)| < \delta$$

Consequently, for every $n > \max(N_1, N_2)$ and every θ and ϕ it holds that

$$|h_n(\theta, \phi) - h(\theta, \phi)| < (M_1 + M_2)\delta + \delta^2$$

Now, given $\epsilon > 0$, we can choose δ small enough so that the right-hand side of the last inequality is smaller than ϵ. That completes the proof of the lemma.

Since $r_n(\theta, \phi)$ converge uniformly to $r(\theta, \phi)$, from (59-60) we see according to the above lemma that $f_n(\theta, \phi)$ converge uniformly to $f(\theta, \phi)$. It implies, together with (61), that for any $\epsilon > 0$ there exists N such that for all $n > N$

$$|V_n - V| < \int_{\theta=0}^{\pi} \int_{\phi=0}^{2\pi} \frac{\epsilon}{4\pi} \sin\theta d\theta d\phi = \epsilon$$

We have thus shown that V_n converge to the actual volume V. It can be easily seen that this reasoning can be extended to higher order moments. That really means that the proposed method can be used to calculate moments of all star-shaped object that occur in practice, because we can approximate a boundary of any real object by a continuously differentiable function such that the error in the particular moment of interest is as small as we wish.

Now let us turn to the surface area. As we can see from (31-34), the expression for the surface area contains r, $\frac{\partial r}{\partial \theta}$, and $\frac{\partial r}{\partial \phi}$. The operations are addition, multiplication and calculation of square root. Similarly to how we proved the lemma above, it can be shown that addition and taking a square root preserve the uniform convergence property. Suppose that A_n is the result of the right-hand side in eq. (34) when we substitute r_n for r, the truncated spherical harmonic series of $\frac{\partial r}{\partial \theta}$ for $\frac{\partial r}{\partial \theta}$ (retaining terms up to the order $l = n$), and the truncated spherical harmonic series of $\frac{\partial r}{\partial \phi}$ for $\frac{\partial r}{\partial \phi}$. It then follows that if $\frac{\partial r}{\partial \theta}$ and $\frac{\partial r}{\partial \phi}$ are continuously differentiable, the sequence of expressions under the integral sign converges

uniformly to $\sqrt{B_1^2 + B_2^2 + B_3^2}$. Consequently, we can apply the above proof to show that A_n converges to A. It remains to show that the spherical harmonic series of r can be differentiated term by term, i.e. the truncated spherical harmonic series of $\frac{\partial r}{\partial \theta}$ and $\frac{\partial r}{\partial \phi}$ can be obtained by differentiating r_n, as we did in Section 4.1. This can be done using integration by parts. Therefore, the sequence of surface areas computed from $r_n(\theta, \phi)$ converges to the actual surface area A.

Furthermore, Orszag [16] has shown that the rate of convergence of spherical harmonic series expansion is determined by the measure of smoothness of $r(\theta, \phi)$. Specifically, if the dericatives of $r(\theta, \phi)$ are continuous up to order p, then R_{lm} goes to zero as $[1/l(l+1)]^p$. For an infinitely differentiable $r(\theta, \phi)$, R_{lm} tends to zero faster than any finite power of $1/l$.

If, however, the function $r(\theta, \phi)$ has discontinuities, the partial sums $r_n(\theta, \phi)$ of a spherical harmonic series exhibit a substantial overshoot near the discontinuity points. The overshoot has a constant height and moves towards the discontinuity contours as the number of terms increases. The effect is referred to as the Gibbs phenomenon. Therefore, for objects with discontinuities the sequence of surface areas may converge to a value different from the actual surface area.

6 Experiments

We wrote a MATLAB program to compare the properties found via our formulas to those calculated by conventional methods in the spatial domain. Two dimensional integration was carried out as follows. The partition of the θ-axis was non-uniform: the density of points at the equator was higher than at the poles since the contribution from each latitude is weighted by $\sin\theta$. The ϕ-axis was divided into 512 equal segments. First we performed integration over θ. The results were then integrated over ϕ. Integration along each axis was done using

a simple trapezoidal method.

Figure 2: Mannequin head

Among the several objects tested was the mannequin head shown in Figure 2. Figures 3-4 present the moments of the mannequin head as a function of the maximum order l of the coefficients retained in the expansion, in reference to the directly computed values. As we can see from the graphs, the values of the moments converge rapidly: truncating the spherical harmonic series at $l = 8$ was sufficient to achieve 99% accuracy.

The results of the calculations by both methods are summarized in Table 1. Note that M_x and M_{xx} have the largest error. To understand this, note that the x-axis was set to be parallel to the base-plane and in the direction of the nose. Consequently, fine face features manifest themselves as rapid variations in the x-coordinate. Thus, the surface has more high-frequency content in terms of the x-coordinate than in y and z. More coefficients are therefore required to represent the variations in the x-direction with a given accuracy. In addition, the coefficients associated with the x-coordinate are more sensitive to errors caused by the finite integration step.

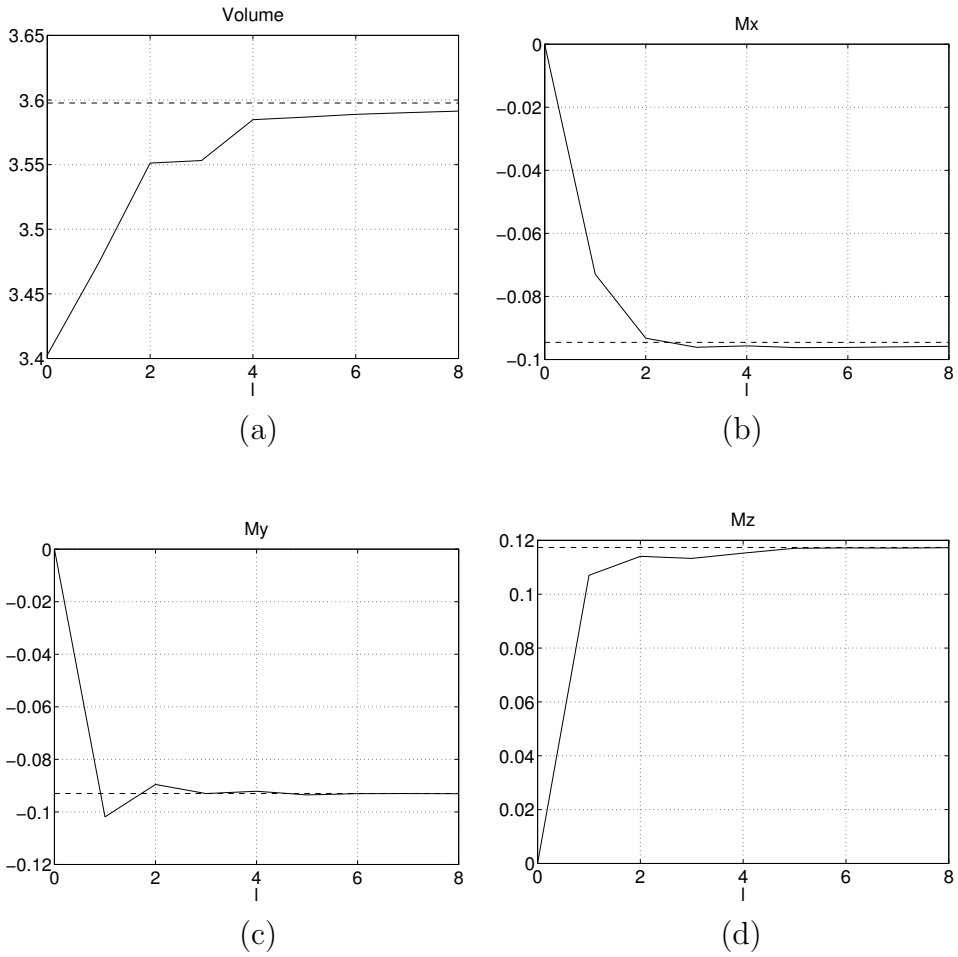

Figure 3: Volume and centroid of the head model as a function of l - the maximum order of the coefficients retained in the expansion: (a) Volume; (b) M_x; (c) M_y; (d) M_z. Dashed line: direct computation; solid line: computation using spherical harmonic coefficients.

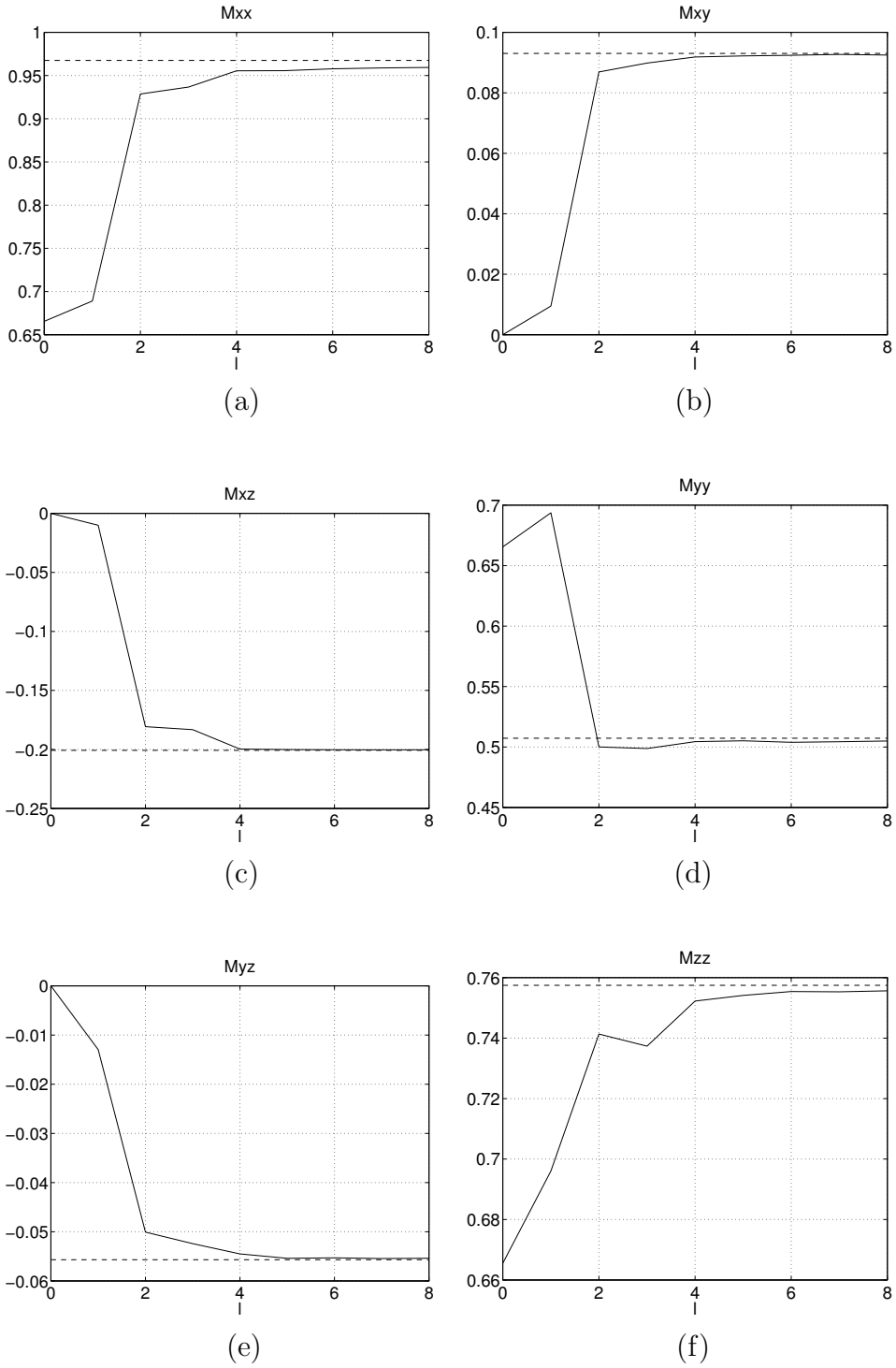

Figure 4: Second-order moments of the head model as a function of l - the maximum order of the coefficients retained in the expansion: (a) M_{xx}; (b) M_{xy}; (c) M_{xz}; (d) M_{yy}; (e) M_{yz}; (f) M_{zz}. Dashed line: direct computation; solid line: computation using spherical harmonic coefficients.

Moment type	Direct Calculation	Spherical Harmonics for $l = 8$	Error (%)
V	3.5977	3.5914	0.1747
M_x	-0.0945	-0.0958	1.3457
M_y	-0.0930	-0.0931	0.0828
M_z	0.1174	0.1173	0.0770
M_{xx}	0.9675	0.9594	0.8345
M_{xy}	0.0930	0.0925	0.5843
M_{xz}	-0.2007	-0.2003	0.2343
M_{yy}	0.5073	0.5050	0.4533
M_{yz}	-0.0557	-0.0554	0.5321
M_{zz}	0.7575	0.7556	0.2403

Table 1: Volume, location of the centroid, and second order moments of the head model.

Referring to the surface area, a lower bound of 11.2 was obtained using the partition

$$\Omega_{mn} = \left\{ m\frac{\pi}{2} \leq \theta < (m+1)\frac{\pi}{2}, \quad n\frac{\pi}{2} \leq \phi < (n+1)\frac{\pi}{2} \right\} \qquad (0 \leq m \leq 1,\, 0 \leq n \leq 3\ )$$

The upper bound was 14.2. The actual value of the surface area was 13.1, estimated by discretization of (28):

$$A = \sum_i \sum_j \left| [\vec{r}(\theta_{i+1}, \phi_j) - \vec{r}(\theta_i, \phi_j)] \times [\vec{r}(\theta_i, \phi_{j+1}) - \vec{r}(\theta_i, \phi_j)] \right|$$

We also tested our method on the near-Earth asteroid, 433 Eros. The NEAR-Shoemaker Laser Rangefinder spacecraft [20] measured Eros' surface height by firing a laser pulse at Eros every second and recording how long it took the beam to reflect from the surface. From these data scientists have built the first detailed maps and three-dimensional model of an asteroid. The website accompanying Zuber et al. [20] provides both the spherical harmonic coefficients of the asteroid, and its volume and moments obtained by direct calculation. We computed the volume and moments of inertia via the spherical harmonic coefficients, and compared them to the reference data provided. The asteroid was assumed

to have a uniform density of 2.67 g/cm^3 [2]. As seen in Table 2, the correspondence between the two results is very good, except for the I_{xz} and I_{yz} moments. Figures 5-6 show how the volume and moments of inertia converge as the number of spherical harmonics used in the expansion is increased. By comparing these graphs with Table 2, we can note that the moments with the largest error, I_{xz} and I_{yz}, are also the slowest to converge. They approach their final values at $l = 13$ while for the other moments $l = 7$ is sufficient. In other words, I_{xz} and I_{yz} are more affected by the fine shape properties. Besides the fact that high-order spherical harmonic coefficients are generally less accurate, direct measurement of these moments is also more prone to errors. The relation between convergence rate and error is therefore expected.

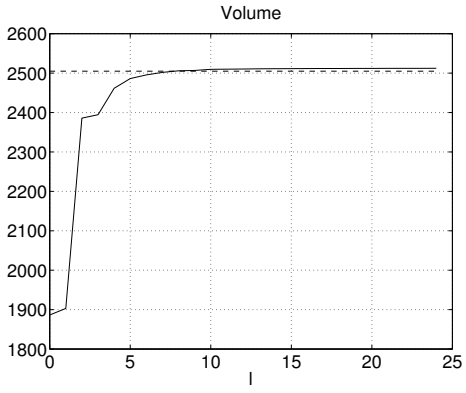

Figure 5: 433 Eros volume in km^3 as a function of l - the maximum order of the coefficients retained in the expansion: Dashed line: original value; solid line: computation using spherical harmonic coefficients.

To explain the 14% difference in the asteroid's I_{xz}, we checked the sensitivity of the features to variations in the spherical harmonic coefficients for both the head and the asteroid. For a small perturbation, the dependence of a moment on some coefficient is approximately linear. Therefore, if we alter each of the coefficients R_{lm} by the amount ΔR_{lm}, a moment I changes by

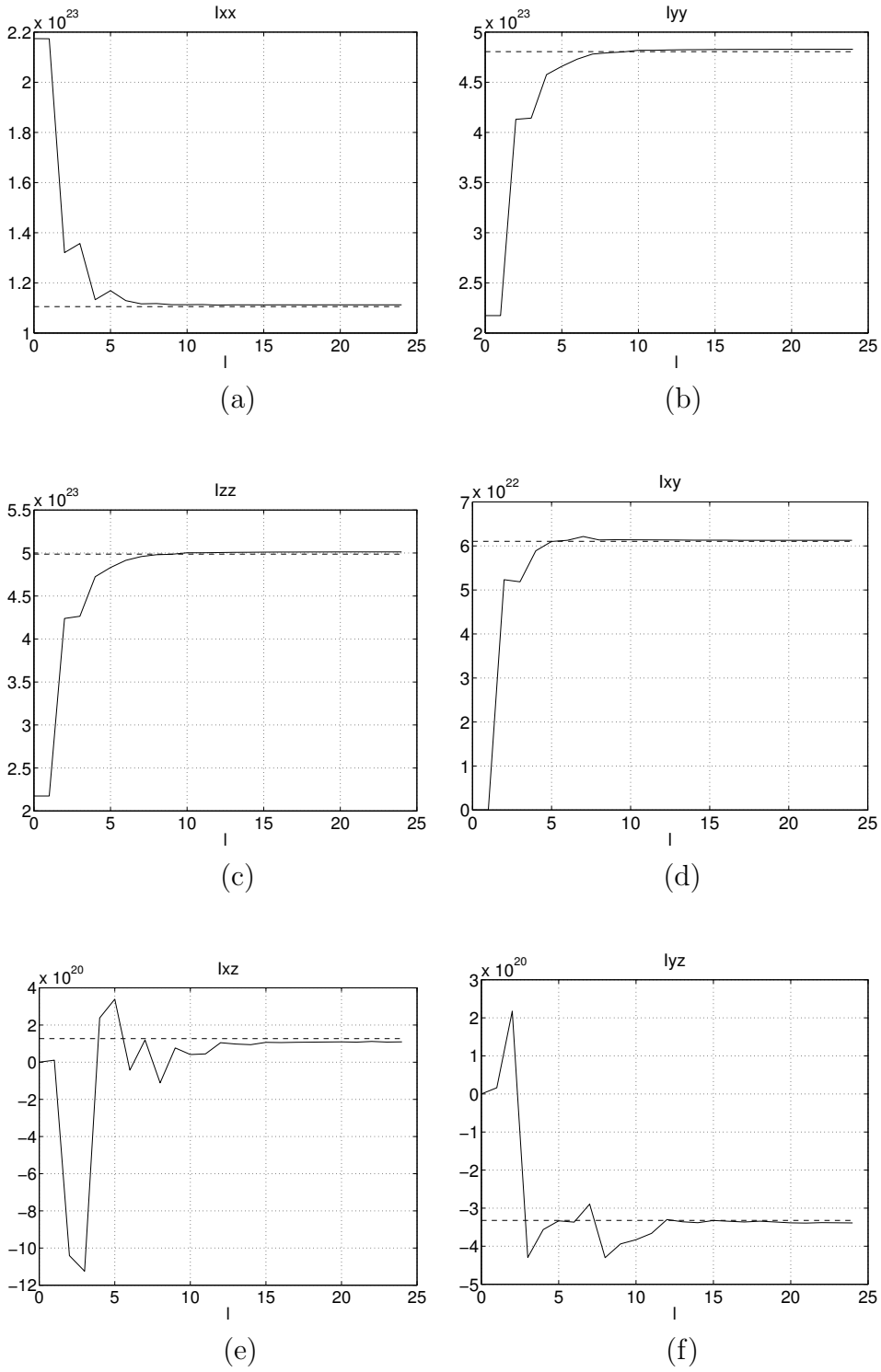

Figure 6: 433 Eros moments of inertia in kg m^2 as a function of l - the maximum order of the coefficients retained in the expansion: (a) I_{xx}; (b) I_{yy}; (c) I_{zz}; (d) I_{xy}; (e) I_{xz}; (f) I_{yz}. Dashed line: original value; solid line: computation using spherical harmonic coefficients.

Moment type	Original Value	Spherical Harmonics	Error (%)
V	2,505	2,512	0.3
I_{xx}	1.1054×10^{23}	1.1125×10^{23}	0.6
I_{yy}	4.8051×10^{23}	4.8296×10^{23}	0.5
I_{zz}	4.9875×10^{23}	5.0131×10^{23}	0.5
I_{xy}	6.1056×10^{22}	6.1276×10^{22}	0.4
I_{xz}	1.2671×10^{20}	1.0936×10^{20}	13.7
I_{yz}	3.3212×10^{20}	-3.3891×10^{20}	2.0 *

Table 2: 433 Eros volume and moments of inertia. The units of the volume are km^3 and the units of moments of inertia are kg m^2. Original value: taken from [20]; spherical harmonics: derived from the spherical harmonic coefficients given on the website accompanying [20]. * We believe that the sign difference in I_{yz} is due to a misprint on the website [20].

$$\Delta I \simeq \sum_{l,m} \frac{\partial I}{\partial R_{lm}} \Delta R_{lm}$$

We systematically changed each coefficient by 1% (one at a time) and experimentally checked the effect. We then calculated two measures of sensitivity. The first is the maximum error caused by a single coefficient change:

$$\Delta I_{\text{single}} = 1\% \cdot \max_{l,m} \left| \frac{\partial I}{\partial R_{lm}} R_{lm} \right|$$

The second corresponds to the situation when all coefficients are changed altogether and the sign of each error is chosen in such a way that the contributions from all coefficients add up in the same direction:

$$\Delta I_{\text{sum}} = 1\% \cdot \sum_{l,m} \left| \frac{\partial I}{\partial R_{lm}} R_{lm} \right|$$

The results of the sensitivity analysis for the head and the asteroid appear in Tables 3 and 4, respectively. As we can see from those tables, the asteroid's I_{xz} is much less stable than all other moments. A one-percent deviation in a single coefficient will cause up to a 20.5%

Moment type	ΔI_{single} (%)	ΔI_{sum} (%)
V	2.9	3.0
M_x	2.6	4.2
M_y	3.0	4.3
M_z	2.8	4.1
M_{xx}	4.4	5.1
M_{xy}	3.5	5.2
M_{xz}	3.4	5.2
M_{yy}	4.9	5.6
M_{yz}	3.0	5.2
M_{zz}	4.6	5.1

Table 3: Sensitivity of the volume, location of the centroid and second order moments to variations in the spherical harmonic coefficients for the head model.

Moment type	ΔI_{single} (%)	ΔI_{sum} (%)
V	2.3	3.0
I_{xx}	4.0	5.1
I_{yy}	2.9	5.0
I_{zz}	2.9	5.0
I_{xy}	2.8	5.4
I_{xz}	20.5	146.0
I_{yz}	3.3	27.4

Table 4: Sensitivity of the volume and moments of inertia to variations in the spherical harmonic coefficients for the 433 Eros asteroid.

change in I_{xz}. Since the one-percent error is well within the accuracy range of the first few coefficients specified in [20], we conclude that the error in I_{xz} is within the expected range.

7 Extension to Objects that are not Star-Shaped

So far our discussion has been limited to star-shaped objects. As we have mentioned previously, not all objects can be described by a radial surface function $r(\theta, \phi)$ since, in general, a radius-vector can cross an object surface at more than one point. However, from topology it is known that any closed surface without holes can be deformed into a sphere by a continuous, one-to-one mapping. Such surfaces are said to be of genus 0. They can be represented

in a parametric form as

$$\vec{r}(\theta,\phi) = x(\theta,\phi)\hat{x} + y(\theta,\phi)\hat{y} + z(\theta,\phi)\hat{z} \tag{62}$$

where $0 \leq \theta \leq \pi$, $0 \leq \phi \leq 2\pi$. It should be emphasized that θ and ϕ here are not necessarily the latitude and the azimuth of the boundary point. When an object surface is given as a collection of points (x_i, y_i, z_i), we need to assign spherical coordinates (θ_i, ϕ_i) to each point. Spherical parameterization is usually formulated as an optimization problem that minimizes some measure of the distortion of the surface net in the mapping. In [1] the objective functional to be maximized is the sum of cosines of four sides over all faces on the sphere corresponding to elementary squares on the original surface. There are also two additional constraints: (i) any object surface region must map to a region of proportional area on the sphere, and (ii) no angle of any spherical quadrilateral must become negative or exceed π. The algorithm that was originally developed in [4] and later extended and applied to surface analysis in [7] uses a functional quantifying the discrepancy between geodesic distances between a set of points on the surface and the corresponding distances on the sphere.

Once we have the spherical parameterization (62), we can expand $x(\theta,\phi)$, $y(\theta,\phi)$, and $z(\theta,\phi)$ in a series of spherical harmonics. Let $\{X_{lm}\}$, $\{Y_{lm}\}$, and $\{Z_{lm}\}$ denote the respective sets of spherical harmonic coefficients. In this section we shall show that the moments and bounds on the surface area can be extracted directly from $\{X_{lm}\}$, $\{Y_{lm}\}$, and $\{Z_{lm}\}$.

For illustration we start with the 2D case. Let us calculate the area of a curve described by $\vec{r}(\phi)$, where $0 \leq \phi \leq 2\pi$ is some parameter. Given $0 \leq \alpha \leq 1$, we denote by $A(\alpha)$ the area of the curve $\alpha\vec{r}(\phi)$ (see Figure 7). The difference between $A(\alpha + d\alpha)$ and $A(\alpha)$ is the area enclosed between $\alpha\vec{r}(\phi)$ and $(\alpha + d\alpha)\vec{r}(\phi)$. We divide this area into

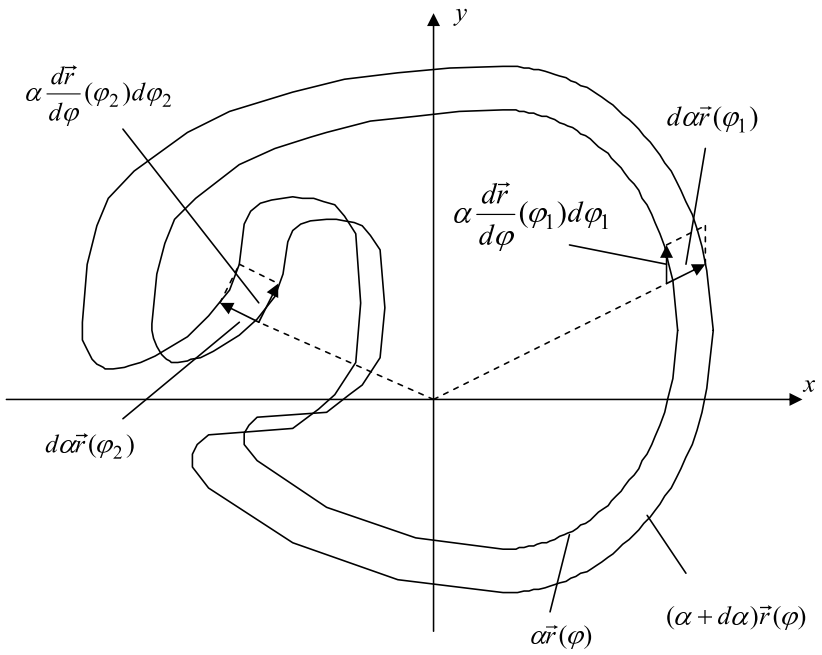

Figure 7: Illustration of Area Calculation for a 2D Non-Star-Shaped Object

infinitesimal parallelograms, each one defined by points $\alpha\vec{r}(\phi)$, $\alpha\vec{r}(\phi + d\phi)$, $(\alpha + d\alpha)\vec{r}(\phi)$, and $(\alpha + d\alpha)\vec{r}(\phi + d\phi)$. The contribution of such a parallelogram to the total area can be expressed as a vector product

$$d\vec{a} = d\alpha\vec{r} \times \alpha\frac{d\vec{r}}{d\phi}d\phi$$

It can be either positive or negative. For example, at $\phi = \phi_1$ the point enters the region as α is increased. The angle from $d\alpha\vec{r}(\phi_1)$ to $\alpha\frac{d\vec{r}}{d\phi}(\phi_1)d\phi_1$ is less than 180^o, so $d\vec{a}$ points in the positive z-direction. On the other hand, at $\phi = \phi_2$ the point leaves the region as α is increased. The angle from $d\alpha\vec{r}(\phi_2)$ to $\alpha\frac{d\vec{r}}{d\phi}(\phi_2)d\phi_2$ is greater than 180^o, so $d\vec{a}$ points in the negative z-direction. It follows that the area of the curve is given by

$$A = \left| \int_{\alpha=0}^{1} \int_{\phi=0}^{2\pi} d\alpha\vec{r} \times \alpha \frac{d\vec{r}}{d\phi} d\phi \right| = \frac{1}{2} \left| \int_{\phi=0}^{2\pi} \vec{r} \times \frac{d\vec{r}}{d\phi} d\phi \right|$$

Now we return to the 3D case. To calculate the moments of a figure given by (62), let us imagine that the object surface is inflated from the origin to its final size in such a way that the intermediate surface $S(\alpha)$ is described by $\alpha\vec{r}(\theta, \phi)$, $0 \leq \alpha \leq 1$. Next divide the region of space enclosed between $S(\alpha)$ and $S(\alpha + d\alpha)$ into infinitesimal parallelepipeds with edges determined by $\alpha \frac{\partial \vec{r}}{\partial \theta} d\theta$, $\alpha \frac{\partial \vec{r}}{\partial \phi} d\phi$, and $d\alpha\vec{r}$. The volume of such a parallelepiped can be written as a triple scalar product

$$dv = \left(\alpha \frac{\partial \vec{r}}{\partial \theta} d\theta \times \alpha \frac{\partial \vec{r}}{\partial \phi} d\phi \right) \cdot d\alpha\vec{r}$$

Note that dv can be both positive and negative. This can be understood as follows. If some radius vector crosses the object surface several times, the points on it are also taken into account more than once. As the object surface is inflated, each time a point enters the object it is taken with a positive sign, and each time a point comes out of the object, it is taken with a negative sign. The points inside the surface are counted an odd number of times, for a net count of 1, whereas the points outside of the surface are counted an even number of times, for a net count of 0. Therefore, the moments of the figure are given by

$$M_{ijk} = \int_{Object} x^i y^j z^k dv$$

$$= \int_{\alpha=0}^{1} \int_{\theta=0}^{\pi} \int_{\phi=0}^{2\pi} (\alpha x)^i (\alpha y)^j (\alpha z)^k \left(\alpha \frac{\partial \vec{r}}{\partial \theta} d\theta \times \alpha \frac{\partial \vec{r}}{\partial \phi} d\phi \right) \cdot d\alpha\vec{r}$$

$$= \frac{1}{i+j+k+3} \int_{\theta=0}^{\pi} \int_{\phi=0}^{2\pi} x^i y^j z^k \left(\frac{\partial \vec{r}}{\partial \theta} \times \frac{\partial \vec{r}}{\partial \phi} \right) \cdot \vec{r} d\theta d\phi \tag{63}$$

Expressing the triple scalar product as a determinant yields

$$M_{ijk} = \frac{1}{i+j+k+3} \int_{\theta=0}^{\pi} \int_{\phi=0}^{2\pi} x^i y^j z^k \begin{vmatrix} x & y & z \\ x_\theta & y_\theta & z_\theta \\ x_\phi & y_\phi & z_\phi \end{vmatrix} d\theta d\phi \tag{64}$$

To validate the above formula, we took as an example a sphere of a unit radius whose center is shifted from the origin to the point (x_0, y_0, z_0). The parameterization is then very simple:

$$x(\theta, \phi) = x_0 + \sin\theta \cos\phi$$

$$y(\theta, \phi) = y_0 + \sin\theta \sin\phi$$

$$z(\theta, \phi) = z_0 + \cos\theta$$

It is easy to see that substituting this into (64) with $i = j = k = 0$ gives the volume of $4\pi/3$, as expected. It can also be shown that if θ and ϕ are the latitude and the azimuth of the boundary point, then (64) reduces to the well-known formula for star-shaped regions.

Now let us denote the integrand in eq. (64) by $F(\theta, \phi)$. Assuming that we know its spherical harmonic coefficients, $\{F_{lm}\}$, we can write the moments of an object in the form

$$M_{ijk} = \frac{1}{i+j+k+3} \int_{\theta=0}^{\pi} \int_{\phi=0}^{2\pi} \left[\sum_{l=0}^{\infty} \sum_{m=-l}^{l} F_{lm} Y_{lm}(\theta, \phi) \right] d\theta d\phi$$

Using the definition in (50) and taking into account that $I_{lm}(\Omega) \neq 0$ only for $m = 0$, we obtain

$$M_{ijk} = \frac{1}{i+j+k+3} \sum_{l=0}^{\infty} F_{l,0} I_{l,0}(\Omega) \tag{65}$$

To calculate $\{F_{l,0}\}$ recall that in Section 4.1 we saw how the spherical harmonic coefficients of $r_\theta \sin\theta$ and r_ϕ can be obtained from those of r by means of a 3D convolution. Using the same technique, we can express the spherical harmonic coefficients of $G(\theta,\phi) = F(\theta,\phi)\sin\theta$ in terms of $\{X_{lm}\}$, $\{Y_{lm}\}$, and $\{Z_{lm}\}$. We shall denote them by $\{G_{lm}\}$. The spherical harmonic coefficients of $h(\theta,\phi) = \frac{1}{\sin\theta}$ can be written according to (4) as

$$H_{lm} = \int_{\theta=0}^{\pi} \int_{\phi=0}^{2\pi} Y_{lm}^*(\theta,\phi) d\theta d\phi$$

It can be seen that $H_{lm} \neq 0$ only for $m = 0$. Finally, applying the 3D convolution theorem (7) to $F(\theta,\phi) = \frac{G(\theta,\phi)}{\sin\theta}$ yields

$$F_{l,0} = \sum_{l_1=0}^{\infty} \sum_{l_2=0}^{\infty} G_{l_1,0} H_{l_2,0}^* \sqrt{\frac{(2l_1+1)(2l_2+1)}{4\pi(2l+1)}} \langle l_1, l_2; 0, 0 | l, 0 \rangle^2 \tag{66}$$

We have thus shown that the moments of a figure can be calculated directly from the spherical harmonic descriptors. In the example of a shifted sphere we saw before,

$$G(\theta,\phi) = \sin^2\theta = \frac{4}{3}\sqrt{\pi} Y_{0,0}(\theta,\phi) - \frac{4}{3}\sqrt{\frac{\pi}{5}} Y_{2,0}(\theta,\phi)$$

In an experiment, we substituted these coefficients into (66) using 50 terms in the expansion of $\frac{1}{\sin\theta}$ to obtain $\{F_{l,0}\}$. Then from (65) we obtained the volume of the unit sphere with error less than 0.1%. As for the surface area, formula (28) is valid for any parameterization

of the form (62), and the rest of the calculations are similar to the above.

However, the numerical stability of this method could be somewhat problematic. Since $G(\theta, \phi)$ is divided by $\sin\theta$ to get $F(\theta, \phi)$, it follows that $G(\theta, \phi)$ tends to zero at least as $\sin\theta$ when θ approaches 0 or π. But if a small error is introduced in the spherical harmonic coefficients $\{G_{lm}\}$, it can be potentially amplified by eq. (66). Therefore we conclude that the star-shaped representation is advantageous, for it is both computationally simpler and more accurate.

8 Complexity Analysis and Transform Method

As one can appreciate, the numerical complexity of our method is determined by the number of operations that need to be performed for calculating spherical harmonic coefficients of a product of two functions. It is apparent from (7) that if $A_{lm} = 0$ and $B_{lm} = 0$ for $l > N$, the total number of operations involved in calculating C_{lm} for each pair l, m scales as N^3. Furthermore, for a Clebsch-Gordan coefficient $\langle l_1, l_2; m_1, m_2 | l, m \rangle$ to be non-zero it is necessary that $l \leq l_1 + l_2$. Consequently, $C_{lm} = 0$ for $l \geq 2N - 1$, i.e. the number of coefficients to be calculated is $O(N^2)$. It follows that $O(N^5)$ arithmetic operations are required to evaluate (7) for all retained l, m. In addition, $O(N^5)$ Clebsch-Gordan coefficients must be calculated off-line and stored somewhere in computer memory. In applications for which the amount of memory required becomes prohibitively large, the Clebsch-Gordan coefficients have to be calculated on the fly. They are usually expressed in terms of the Wigner 3j-symbols [19]. It can then be shown that one Clebsch-Gordan coefficient can be calculated in a linear time. It follows that, in this case, the total computational complexity of (7) for all retained l, m is $O(N^6)$. Our experience shows that spherical harmonic coefficients up to order $l = 15$ are sufficient to represent a typical 3D object with reasonable accuracy.

In this range our method could be substantially faster than the reconstruction of the original object. However, for large N the direct evaluation of (7) is in a too unfavorable competition position with the spatial domain method.

Fortunately, it is possible to evaluate eq. (7) indirectly, by a transform method that does not require knowing the Clebsch-Gordan coefficients [15]. This transform method is based on the fact that if a function $h(\theta, \phi)$ is strictly bandlimited such that $C_{lm} = 0$ for $l \geq b$, then to obtain its spherical harmonic coefficients one does not necessarily have to perform the integral in eq. (4). Instead, it is sufficient to sample $h(\theta, \phi)$ at the equiangular grid of points (θ_j, ϕ_k), $j = 0, \ldots, 2b-1$, $k = 0, \ldots, 2b-1$, where $\theta_j = \pi j/2b$ and $\phi_k = \pi k/b$. It is shown in [5] that h can be recovered from these samples and, furthermore, the spherical harmonic coefficients can be computed in terms of them by the discrete spherical harmonic transform (SHT):

$$C_{lm} = \frac{\sqrt{2\pi}}{2b} \sum_{j=0}^{2b-1} \sum_{k=0}^{2b-1} a_j^{(b)} h(\theta_j, \phi_k) Y_{lm}^*(\theta_j, \phi_k)$$

for $l < b$ and $|m| \leq l$. The weights $a_j^{(b)}$ are determined by solving a system of $2b$ linear equations in $2b$ unknowns. The SHT is calculated using separation of variables. One needs to perform $2b$ discrete Fourier transforms (DFT) and $2b$ discrete Legendre transforms (DLT), each one of length $2b$. The DFT is usually implemented by the fast Fourier transform algorithm whose complexity is $O(b \log b)$. The straightforward evaluation of the DLT has the complexity of $O(b^2)$. With the invention of the fast SHT [5], the complexity of the DLT has been reduced to $O(b \log^2 b)$. Therefore, the SHT can be computed in $O(b^2 \log^2 b)$ time. In a later work [9], an algorithm for the inverse SHT was developed which has the same complexity. Now we can calculate $\{C_{lm}\}$ from eq. (7) with a three-step procedure, just like in the case of a one-dimensional convolution:

(i) reconstruct the values of f from $\{A_{lm}\}$ and g from $\{B_{lm}\}$ at $(2(2N-1))^2$ equiangularly distributed points using the inverse SHT;

(ii) multiply f by g to get the values of h at these points which requires $O(N^2)$ operations;

(iii) compute $\{C_{lm}\}$ from these samples by the SHT.

As we see, the complexity of our method can be made equal to that of the SHT, i.e. $O(N^2 \log^2 N)$.

Since steps (i) and (iii) in the transform method are the inverse of each other, we could optimize our method so that some of the intermediate computations would be saved. For example, to obtain the x-coordinate of the centroid in Section 3, we calculate $\{S_{lm}\}$ from $\{R_{lm}\}$ and then $\{Q_{lm}\}$ from $\{S_{lm}\}$, according to (13-14). If the transform method is used, we perform the SHT on $s(\theta, \phi)$ to get $\{S_{lm}\}$ followed immediately by the inverse SHT on $\{S_{lm}\}$. It is clearly possible to skip these two operations. Moreover, we can first compute the maximum order of the spherical harmonic coefficients in the expansion of the integrand on the right-hand side of (18). Then we reconstruct $r(\theta, \phi)$ at a sufficient number of points and evaluate the integrand at those points. The value of $\bar{x}$ is proportional to the DC coefficient of the integrand. In this way, the calculations are reduced to one SHT and one inverse SHT.

9 Conclusions and Future Work

The representation of star-shaped objects by the spherical harmonic coefficients of their boundary function is used in a variety of scientific domains. In this paper, we explicitly expressed the volume, centroid, second order moments and bounds on the surface area in terms of the spherical harmonic coefficients, without an intermediate reconstruction step. We proved the convergence of the geometric properties, suggested an efficient computational scheme and outlined an extension to genus-0 objects that are not star-shaped. Experiments

with real objects, for which the true values of the geometric properties can be estimated, support the theoretical results.

One direction for further work is motivated by the fact that even with the fast SHT, the complexity of the spherical harmonic method is higher than that of the 2D FFT - $O(N^2 \log N)$. Orszag [16] proposed an alternative expansion for problems in spherical geometry based on special Fourier series. The advantage of the new Fourier series on spheres is that the SHT is replaced there by the regular FFT, so they are computationally simpler. Our preliminary results show that this basis is not inferior to spherical harmonics as far as the efficiency of representing 3D objects is concerned. Future work may also address in more depth the numerical issues of the method for non-star-shaped objects.

APPENDIX

In the Appendix, we shall obtain the expressions for the second-order moments. Proceeding similarly to Section 3.4, we have for the xy-moment

$$M_{xy} = \int_{Object} xy dv = \int_{\rho=0}^{r(\theta,\phi)} \int_{\theta=0}^{\pi} \int_{\phi=0}^{2\pi} (\rho \sin\theta \cos\phi)(\rho \sin\theta \sin\phi)\rho^2 \sin\theta d\rho d\theta d\phi$$

$$= \frac{1}{5} \int_{\theta=0}^{\pi} \int_{\phi=0}^{2\pi} r^5(\theta,\phi)(\sin\theta \cos\phi)(\sin\theta \sin\phi) \sin\theta d\theta d\phi$$

Now we can expand $(\sin\theta \cos\phi)(\sin\theta \sin\phi)$ in a series of spherical harmonics using the 3D convolution theorem (8) with $f(\theta,\phi) = \sin\theta \cos\phi$ and $g(\theta,\phi) = \sin\theta \sin\phi$. Taking into account (21) and (23), we obtain

$$(\sin\theta \cos\phi)(\sin\theta \sin\phi) = C_{2,-2}^{(xy)} Y_{2,-2}(\theta,\phi) + C_{2,2}^{(xy)} Y_{2,2}(\theta,\phi)$$

with the coefficients of the expansion given by

$$C_{2,-2}^{(xy)} = i\sqrt{\frac{\pi}{5}}\,\langle 1,1;0,0|2,0\rangle\,\langle 1,1;-1,-1|2,-2\rangle$$

$$C_{2,2}^{(xy)} = -i\sqrt{\frac{\pi}{5}}\,\langle 1,1;0,0|2,0\rangle\,\langle 1,1;1,1|2,2\rangle$$

Then according to the Parseval theorem (9)

$$M_{xy} = \frac{1}{5}\left(C_{2,-2}^{(xy)*}P_{2,-2} + C_{2,2}^{(xy)*}P_{2,2}\right) \tag{67}$$

As we can see from the last equation, in order to calculate the xy-moment it is sufficient to know the spherical harmonic coefficients of $r^5(\theta,\phi)$ corresponding to $(l,m) = (2,-2)$ and $(2,2)$. The xz-moment can be written in the form

$$M_{xz} = \int_{Object} xz\,dv = \int_{\rho=0}^{r(\theta,\phi)}\int_{\theta=0}^{\pi}\int_{\phi=0}^{2\pi}(\rho\sin\theta\cos\phi)(\rho\cos\theta)\rho^2\sin\theta\,d\rho\,d\theta\,d\phi$$

$$= \frac{1}{5}\int_{\theta=0}^{\pi}\int_{\phi=0}^{2\pi} r^5(\theta,\phi)(\sin\theta\cos\phi)(\cos\theta)\sin\theta\,d\theta\,d\phi$$

Using (8), (21), and (25), we can write $(\sin\theta\cos\phi)(\cos\theta)$ as a linear combination of spherical harmonics:

$$(\sin\theta\cos\phi)(\cos\theta) = C_{2,-1}^{(xz)}Y_{2,-1}(\theta,\phi) + C_{2,1}^{(xz)}Y_{2,1}(\theta,\phi)$$

where

$$C_{2,-1}^{(xz)} = \sqrt{\frac{2\pi}{5}} \langle 1,1;0,0|2,0\rangle \langle 1,1;-1,0|2,-1\rangle$$

$$C_{2,1}^{(xz)} = -\sqrt{\frac{2\pi}{5}} \langle 1,1;0,0|2,0\rangle \langle 1,1;1,0|2,1\rangle$$

Now we apply (9) to get

$$M_{xz} = \frac{1}{5}\left(C_{2,-1}^{(xz)} P_{2,-1} + C_{2,1}^{(xz)} P_{2,1}\right) \tag{68}$$

In a similar way, the yy-moment is given by

$$M_{yy} = \int_{Object} y^2 dv = \int_{\rho=0}^{r(\theta,\phi)} \int_{\theta=0}^{\pi} \int_{\phi=0}^{2\pi} (\rho \sin\theta \sin\phi)^2 \rho^2 \sin\theta d\rho d\theta d\phi$$

$$= \frac{1}{5} \int_{\theta=0}^{\pi} \int_{\phi=0}^{2\pi} r^5(\theta,\phi) (\sin\theta \sin\phi)^2 \sin\theta d\theta d\phi$$

Using (8) and (23), we obtain:

$$(\sin\theta \sin\phi)^2 = C_{0,0}^{(yy)} Y_{0,0}(\theta,\phi) + C_{2,-2}^{(yy)} Y_{2,-2}(\theta,\phi) + C_{2,0}^{(yy)} Y_{2,0}(\theta,\phi) + C_{2,2}^{(yy)} Y_{2,2}(\theta,\phi)$$

where the coefficients of the expansion are given by

$$C_{0,0}^{(yy)} = -2\sqrt{\pi} \langle 1,1;0,0|0,0\rangle \langle 1,1;1,-1|0,0\rangle$$

$$C_{2,-2}^{(yy)} = -\sqrt{\frac{\pi}{5}} \langle 1,1;0,0|2,0\rangle \langle 1,1;-1,-1|2,-2\rangle$$

$$C_{2,0}^{(yy)} = -2\sqrt{\frac{\pi}{5}}\,\langle 1,1;0,0|2,0\rangle\,\langle 1,1;1,-1|2,0\rangle$$

$$C_{2,2}^{(yy)} = -\sqrt{\frac{\pi}{5}}\,\langle 1,1;0,0|2,0\rangle\,\langle 1,1;1,1|2,2\rangle$$

Then, according to the Parseval theorem, we get the following expression for the yy-moment:

$$M_{yy} = \frac{1}{5}\left(C_{0,0}^{(yy)}P_{0,0} + C_{2,-2}^{(yy)}P_{2,-2} + C_{2,0}^{(yy)}P_{2,0} + C_{2,2}^{(yy)}P_{2,2}\right) \tag{69}$$

Next, the yz-moment can be written in the form

$$M_{yz} = \int_{Object} yz dv = \int_{\rho=0}^{r(\theta,\phi)}\int_{\theta=0}^{\pi}\int_{\phi=0}^{2\pi}(\rho\sin\theta\sin\phi)(\rho\cos\theta)\rho^2\sin\theta d\rho d\theta d\phi$$

$$= \frac{1}{5}\int_{\theta=0}^{\pi}\int_{\phi=0}^{2\pi} r^5(\theta,\phi)(\sin\theta\sin\phi)(\cos\theta)\sin\theta d\theta d\phi$$

According to (8), (23), and (25)

$$(\sin\theta\sin\phi)(\cos\theta) = C_{2,-1}^{(yz)}Y_{2,-1}(\theta,\phi) + C_{2,1}^{(yz)}Y_{2,1}(\theta,\phi)$$

where

$$C_{2,-1}^{(yz)} = i\sqrt{\frac{2\pi}{5}}\,\langle 1,1;0,0|2,0\rangle\,\langle 1,1;-1,0|2,-1\rangle$$

$$C_{2,1}^{(yz)} = i\sqrt{\frac{2\pi}{5}}\,\langle 1,1;0,0|2,0\rangle\,\langle 1,1;1,0|2,1\rangle$$

We have from (9)

$$M_{yz} = \frac{1}{5}\left(C_{2,-1}^{(yz)*} P_{2,-1} + C_{2,1}^{(yz)*} P_{2,1}\right) \tag{70}$$

Finally, the zz-moment is given by

$$M_{zz} = \int_{Object} z^2 dv = \int_{\rho=0}^{r(\theta,\phi)} \int_{\theta=0}^{\pi} \int_{\phi=0}^{2\pi} (\rho\cos\theta)^2 \rho^2 \sin\theta d\rho d\theta d\phi$$

$$= \frac{1}{5} \int_{\theta=0}^{\pi} \int_{\phi=0}^{2\pi} r^5(\theta,\phi) \cos^2\theta \sin\theta d\theta d\phi$$

Using (8) and (25), we get

$$\cos^2\theta = C_{0,0}^{(zz)} Y_{0,0}(\theta,\phi) C_{2,0}^{(zz)} Y_{2,0}(\theta,\phi)$$

where

$$C_{0,0}^{(zz)} = 2\sqrt{\pi}\,\langle 1,1;0,0|0,0\rangle^2$$

$$C_{2,0}^{(zz)} = 2\sqrt{\frac{\pi}{5}}\,\langle 1,1;0,0|2,0\rangle^2$$

Finally, according to (9)

$$M_{zz} = \frac{1}{5}\left(C_{0,0}^{(zz)} P_{0,0} + C_{2,0}^{(zz)} P_{2,0}\right) \tag{71}$$

References

[1] Ch. Brechbühler, G. Gerig, and O. Kübler, Parametrization of Closed Surfaces for 3-D Shape Description, *Computer Vision and Image Understanding*, Vol. 61, No. 2, March, pp.154-170, 1995.

[2] D. T. Britt, D. Yeomans, and G. J. Consolmagno, The porosity of 433 Eros, *32nd Lunar and Planetary Science Conference*, March 12-16, 2001, Houston, Texas. Available online at [http://www.lpi.usra.edu/meetings/lpsc2001/pdf/1212.pdf].

[3] C. Cohen-Tannoudji, B. Diu, and F. Lalo, *Quantum Mechanics*, John Wiley & Sons, 1977.

[4] T.F. Cox and M.A.A. Cox, Multidimensional scaling on a sphere, *Communications in Statistics: Theory and Methods*, pp. 2943-2953, Vol. 20, 1991.

[5] J.R. Driscoll and D.M. Healy, Jr., Computing Fourier Transforms and Convolutions on the 2-Sphere, *Advances in Applied Mathematics* 15, pp. 202-250 (1994).

[6] B.S. Duncan, A.J. Olson, Approximation and characterization of molecular surfaces, *Biopolymers* 33 (1993), pp. 219-229.

[7] A. Elad and R. Kimmel, Spherical flattening of the cortex surface, in R. Malladi (ed.), *Geometric Methods in Biomedical Image Processing*, Springer, 2002.

[8] E.J. Garboczi, Three-dimensional mathematical analysis of particle shape using X-ray tomography and spherical harmonics: application to aggregates used in concrete, *Cement and Concrete Research* 32 (2002), pp. 1621-1638.

[9] D. Healy Jr., D. Rockmore, P. Kostelec, and S. Moore, FFTs for the 2-Sphere - Improvements and Variations, *The Journal of Fourier Analysis and Applications*, 9:4 (2003),

pp. 341 - 385. Available on-line at: [http://www.cs.dartmouth.edu/∼geelong/sphere/s2-main.pdf].

[10] W. Kaula, *Theory of Satellite Geodesy*, Dover, New York, 1960; *Geodesy for the Layman, Defense Mapping Agency Technical Report*, 1983. Available at http://geodesy.eng.ohio-state.edu/course/refpapers/NIMA.pdf.

[11] M. Kazhdan, T. Funkhouser and S. Rusinkiewicz, "Rotation invariant spherical harmonic representation of 3D shape descriptors", *Proc. Eurographics Symposium on Geometry Processing*, pp. 156-165, 2003.

[12] Kellogg, Oliver Dimon, *Foundations of Potential Theory*, New York: Ungar, 1970.

[13] N. Kiryati and D. Maydan, Calculating Geometric Properties from Fourier Representation, *Pattern Recognition*, Vol. 22, No. 5, pp. 469-475, 1989.

[14] R. Liboff, *Introductory Quantum Mechanics* (3rd Edition), Addison Wesley, 1998.

[15] S.A. Orszag, Transform Method for the Calculation of Vector-Coupled Sums: Application to the Spectral Form of the Vorticity Equation, *Journal of the Atmospheric Sciences*, Volume 27, pp. 890-895 (1970).

[16] S.A. Orszag, Fourier Series on Spheres, *Monthly Weather Review*, Vol. 102, No. 1, pp. 56-75, January 1974.

[17] D. Saupe and D.V. Vranic, 3D model retrieval with spherical harmonics and moments, *Proceedings Mustererkennung 2001 (DAGM 2001)*, Munich, Sept. 2001. Available online at [http://www.inf.uni-konstanz.de/cgip/bib/files/SaVr01.pdf].

[18] R.B. Schudy and D.H. Ballard, "Towards an anatomical model of heart motion as seen in 4-D cardiac ultrasound data", *Proc. 6th Conf. on Computer Applications in Radiology and Computer-Aided Analysis of Radiological Images*, 1979.

[19] Eric W. Weisstein, "Clebsch-Gordan Coefficient", From MathWorld–A Wolfram Web Resource. http://mathworld.wolfram.com/Clebsch-GordanCoefficient.html

[20] Zuber, M.T., D.E. Smith, A.F. Cheng, J.B. Garvin, O. Aharonson, T.D. Cole, P.J. Dunn, Y. Guo, F.G. Lemoine, G.A. Neumann, D.D. Rowlands, and M.H. Torrence, The Shape of 433 Eros from the NEAR-Shoemaker Laser Rangefinder, *Science*, 289, 1788-1793, 2000. (Additional material for this paper is available at http://www-geodyn.mit.edu/near/nlr.30day.html.)